

# Einstein beams carrying orbital angular momentum

Valeria Rodríguez-Fajardo, Thao P. Nguyen, Kiyon S. Hocek, Jacob M. Freedman, and Enrique J. Galvez

Department of Physics and Astronomy, Colgate University, 13 Oak Drive, Hamilton New York 13346, USA

## ABSTRACT

Einstein beams are coherent optical beams generated by the conditions of gravitational lensing. In the ray picture, Einstein beams are formed by the intersection of light rays deflected by a lensing mass, similar to non-diffracting Bessel beams, but with the difference that adjacent rays diverge slightly. When accounting for the wave properties of light, they form beam-like diffraction patterns that preserve their shape but expand as the light propagates. The addition of a topological charge to the light, leads to more complex patterns carrying orbital angular momentum. For symmetric lensing conditions, Einstein beams carry modes described by confluent hypergeometric functions, which can be approximated by Bessel functions. A theoretical analysis of this is presented here. In astrophysical observations, many of these features can only be inferred because conditions of coherence and alignment make them difficult to observe. Studies of Einstein beams in the laboratory can be used to inform astrophysical observations and discover new non-astrophysical laboratory applications.

**Keywords:** Einstein beams, gravitational lensing, orbital angular momentum

## 1. INTRODUCTION

Light lensed by gravity recombines producing a diffraction pattern. This situation has been investigated since the early days of gravitational lensing.<sup>1,2</sup> Interest in this phenomenon has been thwarted by many challenges in astrophysical lensing observations, such as lack of alignment of the object, lensing mass and Earth; the spatial extent of the source; and fringe averaging over the telescope aperture.<sup>3</sup> Recently we have been able to reproduce all the observable aspects of gravitational lensing in the laboratory.<sup>4</sup> Reproducing lensing in the laboratory was accomplished by deflection of a coherent laser beam with a spatial phase modulator (SLM). The laboratory setup can avoid the challenges of astrophysical observations, coherence, alignment and imaging due to the control that is afforded by laboratory tools. Thus, we were able to observe the diffraction effects of lensing predicted by previous works.

In addition, it has been predicted and measured that lensing from a rotating (Kerr) black hole imparts orbital angular momentum (OAM) to the lensed light.<sup>5,6</sup> This effect has not been included in previous treatments of diffractive lensing effects. In this work we present a theoretical analysis of the diffractive beam bearing OAM.

In Sec. 2 we present the analytical derivation of the Einstein-beam modes bearing OAM, and in Sec. 3 we present images and graphs analyzing the predictions of the theory. Concluding remarks are given in Sec. 4

## 2. MATHEMATICAL MODEL

We want to find a mathematical model that describes how the optical waves evolve as they propagate in space due to gravitational lensing. In strong lensing the distance between objects is much larger than the range over which the light is deflected. For example, for far-away objects at distances of the order of billions of light years, the light is deflected over a distance of the order of thousand of light years.<sup>7</sup> Because of this, we can approximate the deflection to occur instantaneously on a plane. In the same sense, given that observations are carried out very far away from the source and lensing object, we can use the Fresnel approximation<sup>8</sup> in the diffraction of

---

Further author information: (Send correspondence to)

E.J.G: [egalvez@colgate.edu](mailto:egalvez@colgate.edu)

V.R.F: [vrodriquezfajardo@colgate.edu](mailto:vrodriquezfajardo@colgate.edu)

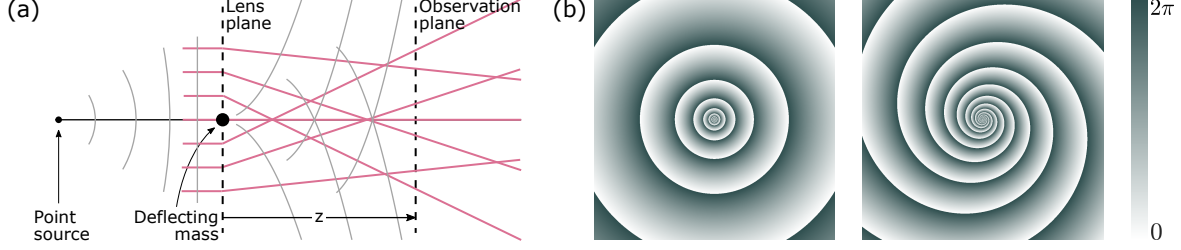


Figure 1. (a) Geometry of the gravitational lensing situation; with the left side not to scale, but representing a far away point source whose rays are nearly parallel by the time they reach the lens plane. (b) The phase phase that is encoded onto the SLM for  $\ell = 0$  (left) and  $\ell = 3$  (right), with the gray level representing the phase modulo  $2\pi$ .

waves. Figure 1(a) shows a schematic of the system to model. The lens confined to a plane deflects the light in the way shown by non-parallel rays and corresponding wavefronts. In polar coordinates, given an initial field  $U_0(r, \theta)$  at the lens plane, after some distance  $z$  (at the observation plane) the field will be

$$U(\rho, \varphi) = \frac{e^{ikz}}{i\lambda z} e^{i\frac{k}{2z}\rho^2} \int_0^\infty \int_0^{2\pi} r U_0(r, \theta) e^{i\frac{k}{2z}r^2} e^{-i\frac{k\rho}{z} \cos(\theta-\varphi)} dr d\theta, \quad (1)$$

where  $\lambda$  is the wavelength,  $k = 2\pi/\lambda$  the wavenumber and  $(r, \theta)$  and  $(\rho, \varphi)$  the coordinates at the lens and observation planes, respectively. Crucially,  $z$  must be strictly greater than zero so the conditions for the Fresnel approximation are fulfilled.

Let's now focus on the lens plane. Light will be deflected depending on the impact parameter  $r$  (the radial coordinate) at an angle<sup>7</sup>

$$\alpha = \frac{2r_S}{r}, \quad (2)$$

where  $r_S = 2GM/c^2$  is the Schwarzschild radius, with  $G$  the gravitational constant,  $M$  the mass of the deflecting object and  $c$  the speed of light. This deflection of the light can be interpreted as phase shifts imparted to the field at the lens plane following<sup>9</sup>

$$\phi = -2kr_S \ln\left(\frac{r}{r_0}\right), \quad (3)$$

where  $r_0$  is a reference value where  $\phi = 0$ . A generalization of this equation is to include the possibility of an azimuthal phase variation of  $2\pi\ell$  around the origin, and where  $\ell$  is an integer known as the topological charge. This type of situation can occur when the lensing object is rotating. In this case, the phase change at the lens plane is

$$\phi = -2kr_S \ln\left(\frac{r}{r_0}\right) - \ell\theta. \quad (4)$$

Figure 1b shows examples of the phase shift introduced by two gravitational lenses, one with no angular momentum ( $\ell = 0$ ) to the left and another with ( $\ell = 3$ ). The effect of  $\ell$  on the phase is clearly seen as the pattern changes from concentric circles to logarithmic spirals.

For phase shifts of the form of Eq. 4 the field just after the lens plane, is given by

$$U_0 = e^{i\phi} = e^{-i\ell\theta} e^{-i2kr_S \ln\left(\frac{r}{r_0}\right)}, \quad (5)$$

where we have assumed a constant unitary field impinging on the lens plane (i.e., a plane wave). Using the natural logarithm properties this equation can be rewritten as,

$$U_0 = r_0^{i2kr_S} r^{-i2kr_S} e^{-i\ell\theta}, \quad (6)$$

which is the optical field we want to propagate. Following Eq. 1, the field at a distance  $z$  is thus

$$U(\rho, \varphi) = \frac{e^{ikz}}{i\lambda z} e^{i\frac{k}{2z}\rho^2} r_0^{i2kr_S} \int_0^\infty \int_0^{2\pi} r^{1-i2kr_S} e^{-i\ell\theta} e^{i\frac{k}{2z}r^2} e^{-i\frac{k\rho}{z} \cos(\theta-\varphi)} dr d\theta. \quad (7)$$

The problem then reduces to solving this integral. We first rearrange the two integrals as

$$U(\rho, \varphi) = \frac{e^{ikz}}{i\lambda z} e^{i\frac{k}{2z}\rho^2} r_0^{i2kr_s} \int_0^\infty r^{1-i2kr_s} e^{i\frac{k}{2z}r^2} \left( \int_0^{2\pi} e^{-i\ell\theta} e^{-i\frac{k\rho}{z}\cos(\theta-\varphi)} d\theta \right) dr \quad (8)$$

$$= \frac{e^{ikz}}{i\lambda z} e^{i\frac{k}{2z}\rho^2} r_0^{i2kr_s} \int_0^\infty r^{1-i2kr_s} e^{i\frac{k}{2z}r^2} I_\theta dr \quad (9)$$

where

$$I_\theta = \int_0^{2\pi} e^{-i\ell\theta} e^{-i\frac{k\rho}{z}\cos(\theta-\varphi)} d\theta. \quad (10)$$

Making the change of variable  $\beta = \theta - \varphi - \frac{\pi}{2}$  and defining  $s = \frac{k\rho r}{z}$ , Eq. 10 becomes

$$I_\theta = e^{-i\ell(\varphi+\frac{\pi}{2})} \int_0^{2\pi} e^{-i\ell\beta} e^{-is\sin\beta} d\beta. \quad (11)$$

whose solution is<sup>10</sup>

$$I_\theta = e^{-i\ell(\varphi+\frac{\pi}{2})} 2\pi J_\ell(s) \quad (12)$$

$$= 2\pi e^{-i\ell(\varphi+\frac{\pi}{2})} J_\ell\left(\frac{k\rho r}{z}\right) \quad (13)$$

where  $J_\ell(\cdot)$  is the Bessel function of the first kind of order  $\ell$ . The propagated field (Eq.8) is therefore

$$U(\rho, \varphi) = \frac{2\pi}{i\lambda z} e^{ikz} e^{i\frac{k}{2z}\rho^2} r_0^{i2kr_s} e^{-i\ell(\varphi+\frac{\pi}{2})} \int_0^\infty r^{1-i2kr_s} J_\ell\left(\frac{k\rho r}{z}\right) e^{i\frac{k}{2z}r^2} dr, \quad (14)$$

which we solved in two different ways, as we describe in detail in the following subsections.

## 2.1 The exact solution

In this section we find the propagated field Eq. 14 by solving the integral exactly. For doing so, we define the parameters

$$\mu = 1 - i2kr_s, \quad \gamma = -i\frac{k}{2z}, \quad b = \frac{k\rho}{z} \quad (15)$$

so that the integral is rewritten as

$$I_r = \int_0^b r^\mu e^{-\gamma^2 r^2} J_\ell(br) dr, \quad (16)$$

whose solution is<sup>10</sup>

$$I_r = \frac{b^\ell \Gamma\left(\frac{\ell+\mu+1}{2}\right)}{2^{\ell+1} \gamma^{\frac{\ell+\mu+1}{2}} \Gamma(\ell+1)} {}_1F_1\left(\frac{\ell+\mu+1}{2}; \ell+1; -\frac{b^2}{4\gamma}\right), \quad (17)$$

where  $\Gamma(\cdot)$  and  ${}_1F_1(a; b; c)$  represent the Gamma and confluent hypergeometric functions, respectively. In terms of the original parameters the previous equation becomes

$$I_r = \frac{e^{i\frac{\pi}{4}(\ell+2-i2kr_s)}}{2\ell!} \left(\frac{k}{2z}\right)^{\frac{\ell-2+i2kr_s}{2}} \Gamma\left(\frac{\ell+2}{2} - i\frac{2kr_s}{2}\right) \rho^\ell {}_1F_1\left(\frac{\ell+2}{2} - i\frac{2kr_s}{2}; \ell+1; -i\frac{k}{2z}\rho^2\right). \quad (18)$$

The propagated field is thus

$$U(\rho, \varphi) = \frac{2\pi}{i\lambda z} e^{ikz} e^{i\frac{k}{2z}\rho^2} r_0^{i2kr_s} e^{-i\ell(\varphi+\frac{\pi}{2})} \frac{e^{i\frac{\pi}{4}(\ell+2-i2kr_s)}}{2\ell!} \left(\frac{k}{2z}\right)^{\frac{\ell-2+i2kr_s}{2}} \Gamma\left(\frac{\ell+2}{2} - i\frac{2kr_s}{2}\right) \rho^\ell {}_1F_1\left(\frac{\ell+2}{2} - i\frac{2kr_s}{2}; \ell+1; -i\frac{k}{2z}\rho^2\right). \quad (19)$$

The final field given by Eq. 19 has the azimuthal phase in the term  $\exp[-i\ell\varphi]$ , and thus carry OAM. The term  $\rho^\ell$  forces the center of the pattern to be dark, consistent with containing a phase singularity: a phase vortex of order  $\ell$ . The confluent hypergeometric function is an oscillating function with an amplitude decreasing with  $\rho$ .

The corresponding intensity profile is proportional to

$$I_{\text{exact}} \propto \left| \frac{\rho^\ell}{z^2} {}_1F_1 \left( \frac{\ell+2}{2} - i\frac{2kr_S}{2}; \ell+1; -i\frac{k}{2z}\rho^2 \right) \right|^2, \quad (20)$$

which describes the energy distribution when the field propagates.

## 2.2 The asymptotic solution

The integral in Eq. 14 is of the form of a generalized Fourier integral

$$I = \int_a^b f(r) e^{ixg(r)} dr \quad (21)$$

where  $a, b, x, f(r)$  and  $g(r)$  must be real, and that can be solved using the method of the Stationary phase<sup>11-13</sup> when  $x \rightarrow \infty$ . In our case,  $k$  plays the role of  $x$ ,

$$f(r) = r J_\ell \left( \frac{k\rho}{z} r \right) \quad g(r) = \frac{r^2}{2z} - 2r_S \ln r, \quad (22)$$

and the solution of I is called the asymptotic approximation. In order to find the latter, we first determine the stationary points, this is, the points  $r_0$  for which the phase  $g(r)$  varies slowly. We do this by solving  $g'(r)|_{r_0} = 0$ , which in our particular case yields  $r_0^2 = 2r_S z$ , that since  $r$  can take only positive values reduces to  $r_0 = +\sqrt{2r_S z}$ . The integral then can be approximated by

$$I \approx f(r_0) e^{ikg(r_0)} e^{i\frac{\pi}{4}} \frac{\Gamma(\frac{1}{2})}{2} \left( \frac{2!}{k|g''(r_0)|} \right)^{\frac{1}{2}} \quad (23)$$

where to define certain constants we have made use of  $g''(r)|_{r_0} > 0$ . Following this equation we obtain

$$I_r \approx e^{-i\frac{\pi}{4}} \sqrt{\frac{\pi}{8kr_S}} e^{ikr_S} J_\ell \left( \sqrt{\frac{2k^2 r_S}{z}} \rho \right), \quad (24)$$

therefore the propagated field in the asymptotic approximation becomes

$$U(\rho, \varphi) = \frac{2\pi}{i\lambda z} e^{ikz} e^{i\frac{k}{2z}\rho^2} r_0^{2kr_S} e^{-i\ell(\varphi + \frac{\pi}{2})} e^{-i\frac{\pi}{4}} \sqrt{\frac{\pi}{8kr_S}} e^{ikr_S} J_\ell \left( \sqrt{\frac{2k^2 r_S}{z}} \rho \right), \quad (25)$$

whose intensity is proportional to

$$I_{\text{asymptotic}} \propto \left| J_\ell \left( \sqrt{\frac{2k^2 r_S}{z}} \rho \right) \right|^2, \quad (26)$$

which describes the energy distribution in the asymptotic approximation when the field propagates.

This solution is expressed in terms of the more familiar Bessel function. This calls for a comparison with non-diffracting Bessel beams, as presented next.

## 3. RESULTS AND DISCUSSION

In the next subsections we present comparisons of the calculation of the diffraction pattern carried by Einstein beams done with the exact expression, in terms of confluent hypergeometric functions, and the asymptotic expression, in terms of Bessel functions. We do several comparisons for different lensing masses, expressed in terms of the Schwarzschild radius, as a function of the propagation direction, and as a function of the wavelength of the light. We also show our results for different values of the topological charge for beams bearing OAM.

### 3.1 Schwarzschild radius dependence

Figure 2 is a comparison of images of the Einstein modes for the two types of solutions: the exact one (Eq. 20), in terms of confluent hypergeometric functions, and the approximate asymptotic in terms of Bessel functions (Eq. 25). There are four images for each solution, with the exact solution shown in row (a) and the approximate shown in row (b). They are shown for different values of the Schwarzschild radius while keeping the wavelength constant. Row (c) shows a cut of the intensity across a line that passes through the center of the mode. We can see that there is a small difference in the height of the central peak, with the asymptotic solution always slightly higher. The asymptotic regime sets in when  $r_S \gg 1/k$ , where  $k$  is the wavenumber of the light. In our case  $k = 10^7$ , so the asymptotic regime is not quite set in with  $r_S \sim 10^{-6}$ . Yet, the Bessel function is an easy one to use when describing the beam.

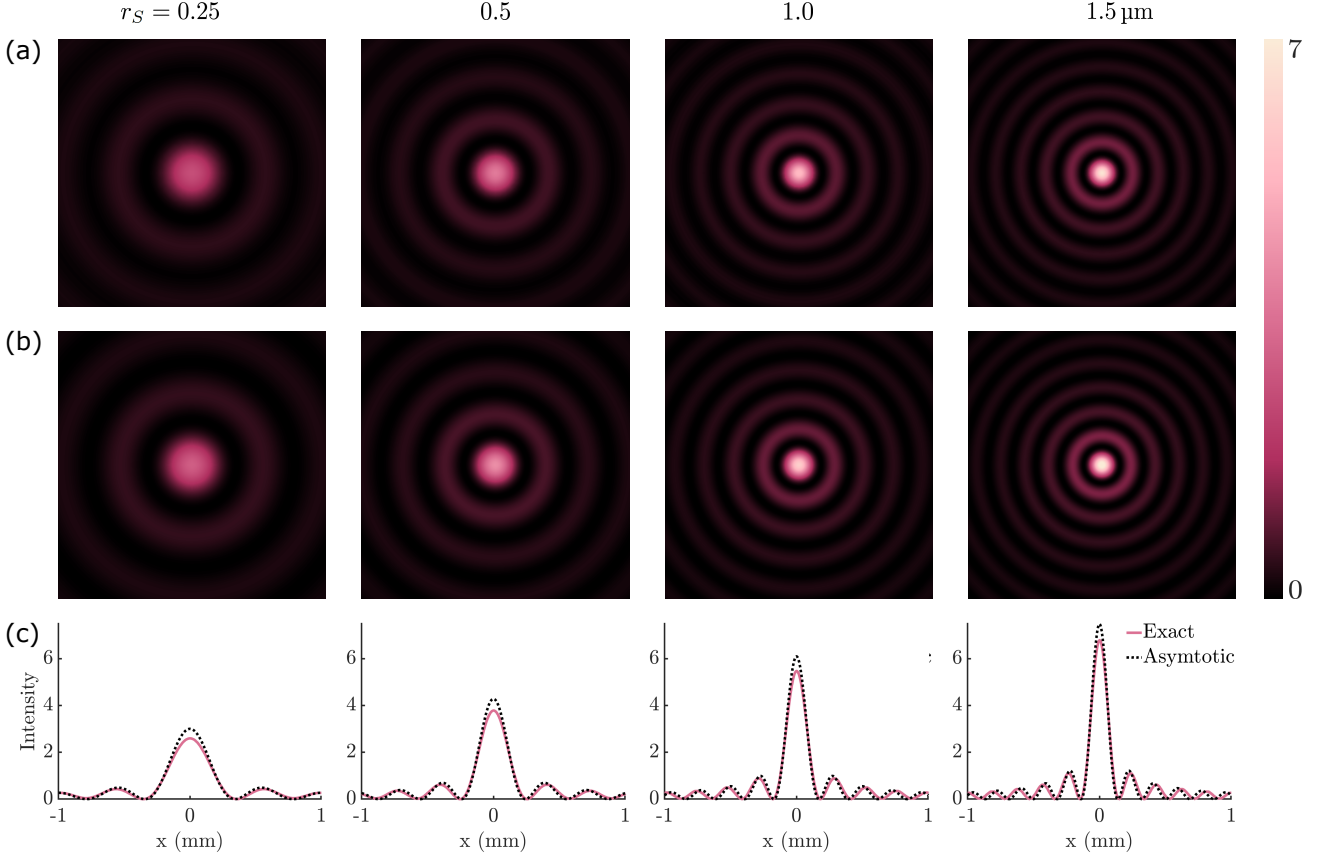


Figure 2. Einstein-beam images calculated via the exact solution (a), asymptotic solution (b) for different values of the Schwarzschild radius of the lensing mass in  $\mu\text{m}$ . (c) Comparison of cuts of the intensity of the patterns through their center.

The figure also shows what may not be so intuitive, that as the mass of the lensing object increases, and consequently the Schwarzschild radius, the pattern shrinks. This can be understood simply in terms of the ray picture, shown in Fig. 5(a): because the deflection angle increases with  $r_S$  (cf. Eq. 2), the deflection angle increases with the lensing mass, compressing the pattern.

### 3.2 Propagation distance dependence

In Fig. 3 we show the dependence of the pattern with the propagation distance  $z$ . This is shown in different ways in parts (a) and (b) of the figure. As  $z$  increases, the pattern increases in size. This is in contrast to non-diffracting Bessel beams, where the size of the pattern remains constant. However, the ideal Bessel beams are infinite because they are produced by infinite plane waves. Laboratory-based Bessel beams occur over a finite

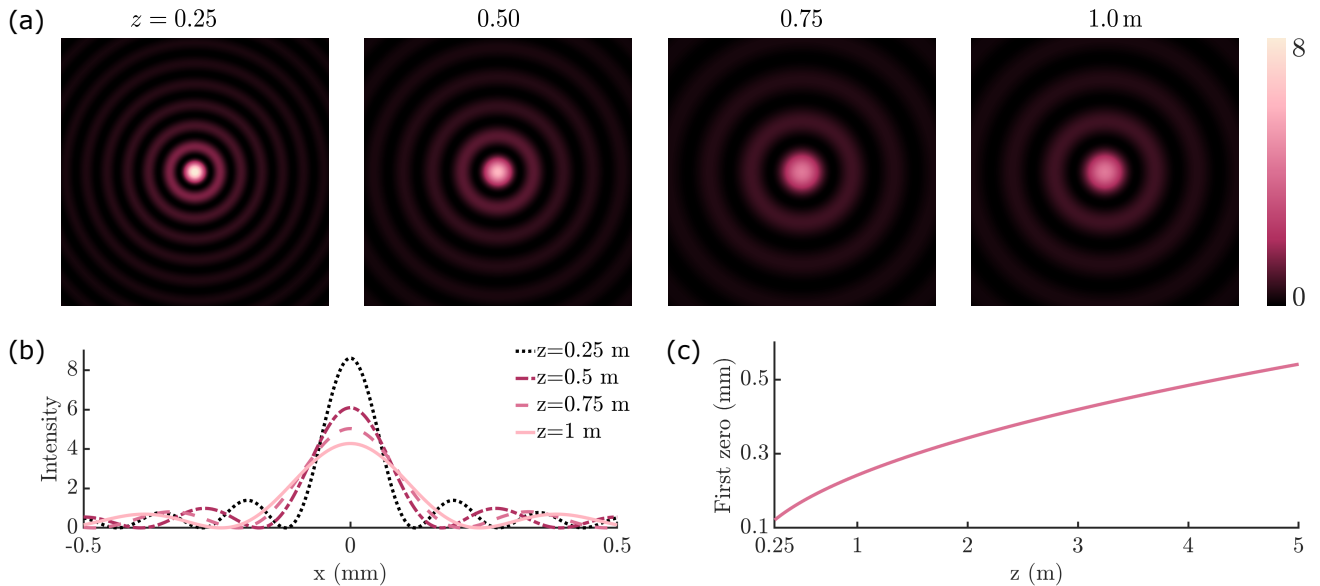


Figure 3. The divergence of the Einstein beam as a function of  $z$  is shown in different ways: images (a), transverse intensity profiles (b), and radius of the first minimum (c).

span over the propagation distance due to the finite size of the beam.<sup>14</sup> In contrast, the Einstein beam continues for much longer owing to the deflection angle decreasing with impact-parameter value, as shown in Fig. 5(a). Its expansion depends on  $\sqrt{z}$ . We can see this by considering the argument of the Bessel beam in the asymptotic solution corresponding to the first zero, where

$$\rho_1 = \frac{2.405\lambda}{2\pi} \sqrt{\frac{z}{2r_S}}, \quad (27)$$

and shown in Fig. 3(c). The angular divergence of the beam decreases as  $z$  increases, in contrast to Gaussian beams where the divergence angle reaches a constant value.

### 3.3 Wavelength dependence

The size of the Einstein beam increases linearly with wavelength, as seen in Eq. 27 by means of the radius of the first zero. In Fig. 4 we show the wavelength dependence in various ways. In 4(a) we show the pattern for 3 different wavelengths: blue (442 nm), green (532 nm) and red (633 nm). We show a transverse cut of the intensity for each wavelength in (c), and a graph of the radius of the first zero as a function of the wavelength in (d).

In the color version of Fig. 4(b) we see the superposition of the patterns with the three wavelengths, showing the dispersion caused by the diffraction of the light.

### 3.4 Orbital angular momentum dependence

One of the main objectives of this work is to study the effect of orbital angular momentum on gravitational diffraction. In Figs. 5(a) and (b) we show the effect of adding orbital angular momentum to the lensed light. In the asymptotic limit this pattern is well explained by a Bessel function of order equal to the topological charge  $\ell$ . For  $\ell \neq 0$  the center of the pattern is a minimum, with the radius of the rings increasing as  $\ell$  increases. The figure shows the monochrome and color versions of the patterns.

The composite patterns show that the patterns with different topological charge disperse the light in different degrees. The patterns use the 3 wavelengths used in Fig. 4. While the three wavelengths appear to overlap for low values of  $\ell$ , they clearly show significant dispersion for higher values of  $\ell$ .

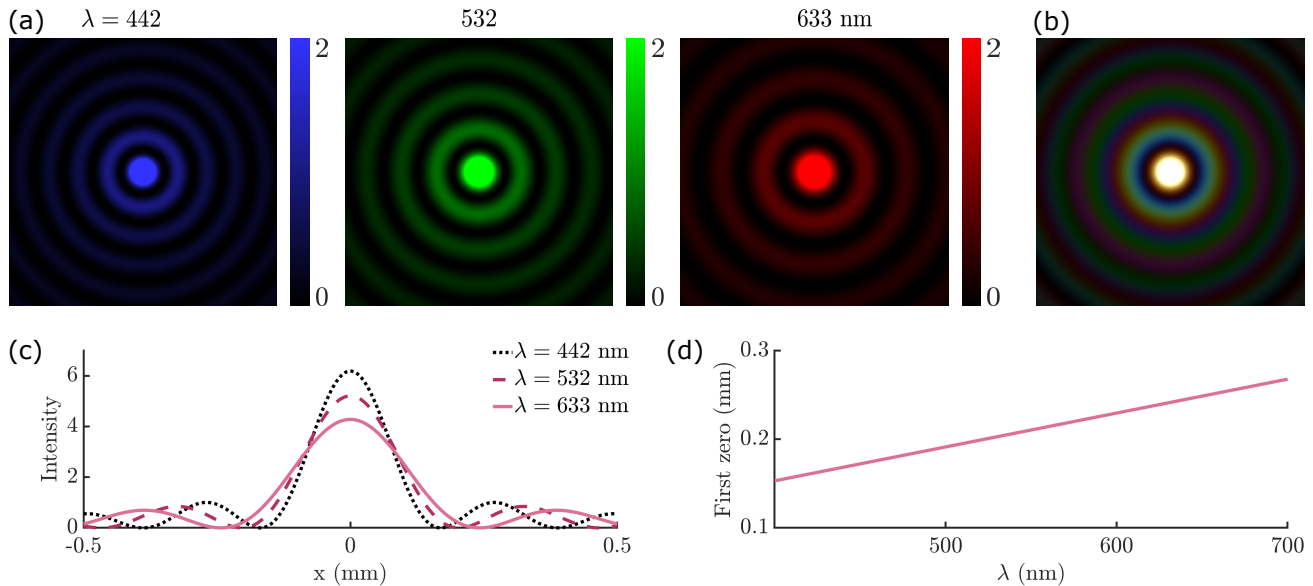


Figure 4. The variation of the Einstein beam pattern with wavelength is shown by the pattern at 3 different wavelengths (a): 442 nm, 532 nm and 633 nm. A superposition of these patterns in (b), and a cut of the intensity as a function of the transverse dimension (c). The radius of the first minimum as a function of the wavelength is shown in (d).

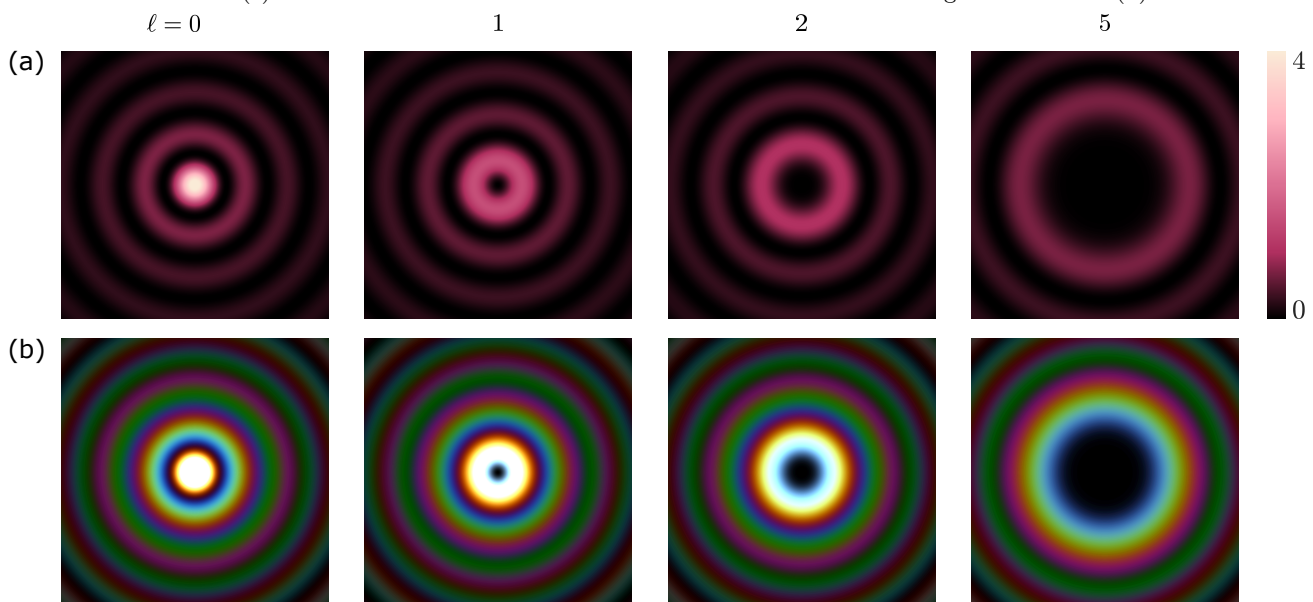


Figure 5. Einstein-beam patterns for different values of the topological charge  $\ell$  for a fixed wavelength (a). The images in (b) show the composite images using 3 different wavelengths: 442 nm, 532 nm and 633 nm.

#### 4. CONCLUSIONS

In summary, we present an analysis of the effect of OAM on the diffraction patterns of gravitational lensing. This type of optical angular momentum is introduced in the laboratory via an azimuthal phase encoded onto the SLM. We present the theoretical analysis of the diffracted beam by propagating the Fresnel integral, which incorporates the azimuthal phase. The resulting Einstein beams indeed show the characteristics of other types of laboratory optical beams that carry OAM, featuring a central dark region containing an optical vortex corresponding to the topological charge of the OAM. In the asymptotic solution, the pattern is described by a Bessel beam of order equal to the topological charge. This is very similar to non-diffracting Bessel beams. The remarkable difference between Einstein beams and Bessel beams is that while Bessel beams have a finite extent due to the finite extent

of the beam diameter, Einstein beams continue to expand as the light propagates. The expansion rate is smaller than the expansion of Gaussian beams, making Einstein beams suitable for other non-astrophysical applications, such as imaging and communications.

## ACKNOWLEDGMENTS

This work was funded by the National Science Foundation grant PHY-2011937.

## REFERENCES

- [1] Bliokh, P. V. and Minakov, A. A., “Diffraction of light and lens effect of the stellar gravitation field,” *Astrophysics and Space Science* **34**(2), L7–L9 (1975).
- [2] Herlt, E. and Stephani, H., “Wave optics of the spherical gravitational lens part i: Diffraction of a plane electromagnetic wave by a large star,” *International Journal of Theoretical Physics* **15**(1), 45–65 (1976).
- [3] Deguchi, S. and Watson, W. D., “Diffraction in gravitational lensing for compact objects of low mass,” *Ap. J.* **307**, 30–37 (1986).
- [4] Rodríguez-Fajardo, V., Nguyen, T. P., Hocek, K. S., Freedman, J. M., and Galvez, E. J., “Einstein beams and the diffractive aspect of gravitationally lensed light,” (2023).
- [5] Harwit, M., “Photon orbital angular momentum in astrophysics,” *The Astrophysical Journal* **597**, 1266–1270 (nov 2003).
- [6] Tamburini, F., Thidé, B., and Valle, M. D., “Measurement of the spin of the M87 black hole from its observed twisted light,” *Monthly Notices of the Royal Astronomical Society* **492**, L22–L27 (Feb. 2020).
- [7] Schneider, P., Ehlers, J., and Falco, E. E., [*Gravitational Lenses*], Springer (1992).
- [8] Goodman, J. W., [*Introduction to Fourier Optics*], W. H. Freeman (2017).
- [9] Galvez, E. J. and Freedman, J. M., “Einstein beams: Optical beams following gravitationally lensed trajectories,” *Proc. SPIE* **11701**, 117010U (2021).
- [10] Gradshteyn, I. S. and Ryzhik, I. M., [*Table of integrals, series, and products*], Academic press (2015).
- [11] Bender, C. M., Orszag, S., and Orszag, S. A., [*Advanced mathematical methods for scientists and engineers I: Asymptotic methods and perturbation theory*], vol. 1, Springer Science & Business Media (1999).
- [12] Born, M., Wolf, E., Bhatia, A. B., Clemmow, P. C., Gabor, D., Stokes, A. R., Taylor, A. M., Wayman, P. A., and Wilcock, W. L., [*Principles of Optics: Electromagnetic Theory of Propagation, Interference and Diffraction of Light*], Cambridge University Press, 7 ed. (1999).
- [13] Copson, E. T., [*Asymptotic Expansions*], Cambridge Tracts in Mathematics, Cambridge University Press (1965).
- [14] Durnin, J., Miceli, J. J., and Eberly, J. H., “Diffraction-free beams,” *Phys. Rev. Lett.* **58**, 1499–1501 (Apr 1987).